Fusion Engineering and Design 217 (2025) 115113

Contents lists available at ScienceDirect

Fusion Engineering and Design

journal homepage: www.elsevier.com/locate/fusengdes

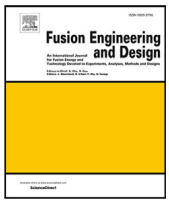

3D magneto-convective instabilities of liquid metal flow in a generic geometry related to WCLL blankets

B. Lyu *, L. Bühler, C. Koehly, C. Mistrangelo

Karlsruhe Institute of Technology (KIT), P.O. Box 3640, 76021 Karlsruhe, Germany

ARTICLE INFO

Keywords:
Magnetohydrodynamics (MHD)
WCLL blankets
Magneto-convective instabilities
Heat transfer

ABSTRACT

The water-cooled lead lithium breeding blanket has been selected as one of the test blanket modules for the International Thermonuclear Experimental Reactor (ITER). In this blanket concept, heat generated by neutron collisions is extracted through water-cooled pipes immersed in the liquid eutectic lead-lithium alloy (PbLi), which serves as both a breeder material and a heat transfer medium. Temperature gradients in PbLi cause buoyancy-driven motion, while Lorentz forces, arising from flow-induced electrical currents in the presence of a magnetic field, act to suppress this motion. A comprehensive understanding of these complex 3D magnetohydrodynamic (MHD) phenomena is essential to assess the feasibility of liquid metal blankets. The present study investigates the convective MHD flow in a simplified model geometry featuring a long rectangular cavity with a coaxial circular cooling pipe maintained at a constant temperature, with imposed uniform volumetric heating in the fluid. Previous numerical simulations for an infinitely long cavity in axial direction reveal magneto-convective motion in transverse planes, where a cold plume “falls down” beneath the cooling pipe. The present 3D study extends previous analyses and identifies a bifurcation and transition from the 2D state to complex 3D flow structures at sufficiently high volumetric heating. The observed convection rolls preferentially align with the transverse horizontal magnetic field and affect significantly the convective heat transfer.

1. Introduction

Liquid metal magnetohydrodynamics is a research field of significant importance in the context of magnetically confined fusion reactors, where liquid metals are employed in divertors and breeding blankets to fulfill critical purposes such as extracting heat from surface loads and volumetric heating, tritium breeding, and radiation shielding. The exceptional thermal conductivity, low viscosity, and high-temperature resilience of liquid metals make them highly attractive for advanced heat transfer and thermal management in fusion systems. However, the interaction of these electrically conductive fluids with intense magnetic fields introduces complex multi-physics phenomena that significantly influence the flow behavior. The competition between buoyancy forces, driven by density gradients, and the damping effects imposed by viscosity and magnetic field determines the structure of convective flow, leading to complex flow dynamics with impact on heat and mass transport properties. Since the mean forced purge flow required for tritium removal in the European water-cooled lead lithium (WCLL) blanket concept [1,2] is very small, buoyancy is expected to be the primary driving mechanism for the flow in breeder units. Therefore, understanding of magneto-convective phenomena is essential for optimizing the performance and efficiency of liquid metal based systems in fusion reactor environments.

Magneto-convective liquid metal flows have been extensively studied both theoretically and experimentally over the last decades. Chandrasekhar’s work [3] applied linear stability theory to determine the onset of convection in an infinitely extended horizontal fluid layer heated from below and subjected to a vertical magnetic field. His analysis revealed that the Rayleigh number, which characterizes the balance between buoyancy and viscous forces, must exceed a critical value for convection to start, with the threshold increasing under the influence of a magnetic field.

Experimental investigations by Burr et al. [4,5] focused on magnetohydrodynamic (MHD) Rayleigh–Bénard convection within a large-aspect-ratio rectangular box and provided valuable insights into how the orientation of magnetic field influences convection patterns. Burr also demonstrated that stronger magnetic fields suppress heat transfer by damping convective motions, thereby reducing the overall heat transfer efficiency.

Numerical studies have further explored mixed convection in pipes and ducts under varying configurations of flow direction, magnetic

* Corresponding author.
E-mail address: biao.lyu@kit.edu (B. Lyu).

https://doi.org/10.1016/j.fusengdes.2025.115113
Received 13 January 2025; Received in revised form 14 April 2025; Accepted 17 April 2025
Available online 6 May 2025
0920-3796/© 2025 Published by Elsevier B.V.

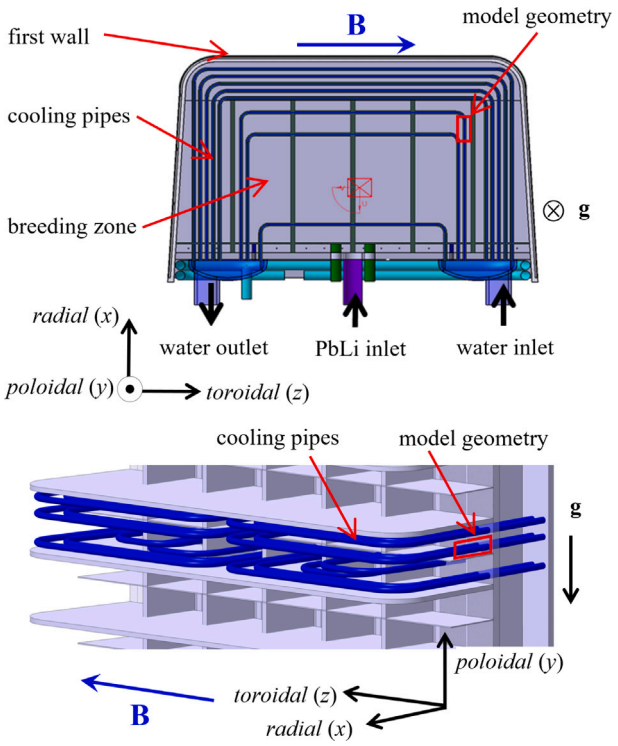

Fig. 1. View of an equatorial cross section of a WCLL blanket (top: early DEMO design by ENEA, bottom: more advanced version by ENEA [10]). The pipes are filled with pressurized water and immersed in the liquid metal PbLi. **B** and **g** are the toroidal component of magnetic field and the gravitational acceleration. The red rectangles indicates the subdomain from which the model geometry is derived.

field orientation, and heat flux, as summarized in the review paper by Zikanov et al. [6]. Despite these a advancements, only a few studies on magneto-convection with volumetric heating and internal obstacles have been published (see *e.g.* [7–9]) showing quite complex flow patters due to a larger number of cooling pipes or spatial dependence of volumetric heating. However, fundamental studies on magneto-convection in closed geometries with uniform volumetric heating and internal obstacles, have received less attention.

This study aims to fill the gap in existing research by examining the fundamental problem of convective MHD flow of a volumetrically heated liquid metal. The flow is confined within a model geometry, consisting of a long rectangular cavity with a coaxial circular cooling pipe maintained at a constant temperature. This setup provides new insights into the interaction between buoyancy-driven convection and magnetic damping in the model geometry by varying in a wide range heating and magnetic field.

The model geometry used in this study is derived from the breeding zone of the WCLL breeding blanket. A view in an equatorial cross section of the current WCLL blanket design [10–12] is presented in Fig. 1. The WCLL blanket consists of a plasma-facing first wall with cooling pipes embedded to manage heat and neutron flux, a breeding zone filled with liquid lithium lead (PbLi) for tritium production and heat absorption, and a back structure for mechanical support and coolant distribution. Highly pressurized water circulates through the C-shaped radial-toroidal-radial pipes to extract heat, while tritium is recovered from PbLi via slow purge flow towards ancillary extraction systems. For the current study, a model geometry (Fig. 2) is selected to focus on a single cooling pipe and the liquid metal in its vicinity, confined within a representative rectangular volume, as illustrated by the small red subdomain in Fig. 1.

The model geometry has a square cross section of nondimensional size 2×2 in y and z directions, when the Hartmann length (half duct

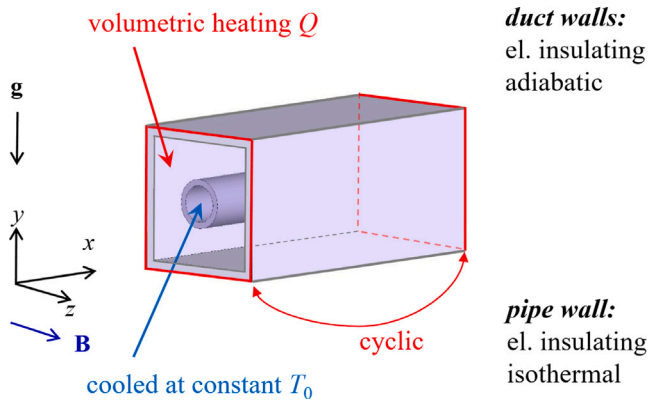

Fig. 2. Model geometry and boundary conditions for numerical simulations. The origin of the coordinate system is located at the center of the cavity.

width along magnetic field lines, where $\mathbf{B} = B\hat{\mathbf{z}}$) is used as typical length scale L. The outer nondimensional diameter of the cooling pipe is 0.66. For the numerical simulations conducted in this study, several idealized boundary conditions have been employed, as depicted in Fig. 2. A uniform volumetric thermal load Q is distributed throughout the liquid metal. The pipe wall is cooled at constant temperature T_0 and modeled as electrically insulating. The duct walls are assumed to be adiabatic and electrically insulating. In axial direction cyclic conditions are applied, representing fully developed or periodic flow in that direction.

Using a simplified model geometry and boundary conditions, this study aims to develop a fundamental understanding of the underlying phenomena and to investigate the effects of magnetic field strength and volumetric heating. It is important to recognize that idealized thermal and electrical boundary conditions significantly influence pattern formation. In addition, although not considered in the present work, the blockage ratio and aspect ratio of the cross section play a critical role in shaping the flow dynamics and deserve future consideration.

2. Governing equations and dimensionless numbers

The dynamics of buoyancy-driven magneto-convective flows are governed by the interaction of fluid dynamics (Navier–Stokes equations), thermodynamics (energy conservation), and electromagnetism (Maxwell's equations). Neglecting displacement currents is a common simplification in liquid metal magnetohydrodynamics when dealing with low-frequency phenomena, such as flow of liquid metals or plasmas. Additionally, the inductionless approximation, which assumes that the magnetic field is entirely unaffected by the flow motion, is frequently employed for liquid metal flows under engineering conditions, where the magnetic Reynolds number is small.

According to [13], the dimensionless equations for momentum conservation, Ohm's law and the heat equation become

$$\frac{\partial \mathbf{u}}{\partial t} + (\mathbf{u}\cdot\nabla)\,\mathbf{u} = -\nabla p + \frac{1}{\sqrt{Gr}}\nabla^2\mathbf{u} + T\hat{\mathbf{y}} + \frac{Ha^2}{\sqrt{Gr}}(\mathbf{j}\times\mathbf{B})\,, \tag{1}$$

$$\mathbf{j} = -\nabla\phi + \mathbf{u}\times\mathbf{B}\,, \tag{2}$$

$$\frac{\partial T}{\partial t} + (\mathbf{u}\cdot\nabla)T = \frac{1}{Pr\sqrt{Gr}}(\nabla T + 1)\,, \tag{3}$$

with conservation of mass $\nabla\cdot\mathbf{u} = 0$ and charge $\nabla\cdot\mathbf{j} = 0$. In these equations $\mathbf{u}$, $\mathbf{B}$, $\mathbf{j}$, ϕ and t denote velocity, magnetic field, current density, electric potential and time, scaled by $u_0 = \sqrt{g\beta\Delta T L}$, B, $j_0 = \sigma u_0 B$, and $u_0 BL$, L/u_0, respectively. Here g denotes gravitational acceleration, β stands for the volumetric expansion coefficient of the liquid metal, and the characteristic temperature difference $\Delta T = QL^2/k$

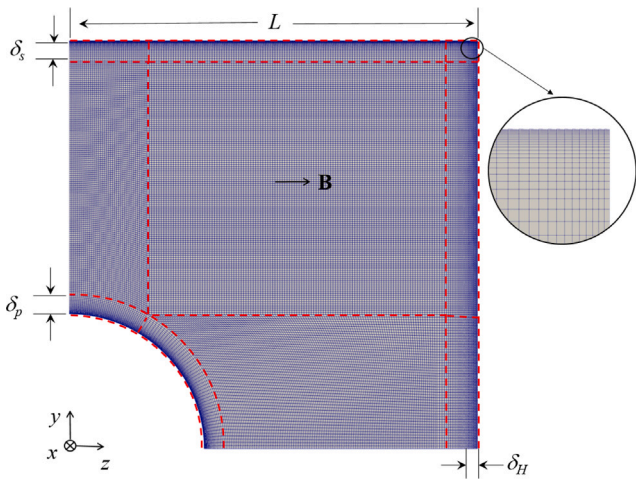

Fig. 3. Sketch of the grid used for the simulations.

is defined by the rate of volumetric heating Q and thermal conductivity of the fluid k. The dimensionless temperature T denotes deviations from the reference T_0 scaled by ΔT.

The flow is governed by the Grashof number Gr, Hartmann number Ha and Prandtl number Pr:

$$Gr = \frac{g\beta\Delta T L^3}{\nu^2},\quad Ha = BL\sqrt{\frac{\sigma}{\rho_0 \nu}},\quad Pr = \frac{\nu}{\kappa}.$$

The Grashof number quantifies the relative significance of buoyancy forces compared to viscous forces. The Hartmann number is a nondimensional measure for the magnetic field and its square quantifies the ratio of electromagnetic forces to viscous forces. The reference density ρ_0 is taken at the reference temperature T_0. The Prandtl number represents the ratio of momentum diffusivity to thermal diffusivity.

For the WCLL blanket under ITER operating conditions, the Hartmann number is approximately 6000, while the Grashof number varies between 2.5×10^{10} and 7.6×10^{10} [14]. Under these extreme conditions, the pronounced damping effect of the Lorentz force inhibits flow motion, which in turn reduces heat transfer efficiency. Simultaneously, the inhomogeneous temperature distribution, resulting from heat transfer at the cooling pipe and volumetric heating in the fluid, promotes the emergence of magneto-convective flow patterns. In order to gain a deeper comprehensive understanding of the phenomena, numerical simulations are systematically performed in this study. The present analysis covers the parameter range $Ha = 200 \div 1000$, $Gr = 3\times10^6 \div 3\times10^9$, where most interesting phenomena such as transition from 2D to 3D flow with increased heat transfer are observed.

3. Numerical results

The governing equations (1)–(3) have been implemented within the open-source computational framework OpenFOAM, employing a cell-centered (collocated) finite volume method. The MHD code used in this study was developed at KIT [15] and is based on the conservative algorithm proposed in [16]. This code has been rigorously validated for example by comparisons with experimental results for magneto-convection around differentially heated cylinders [17] or mixed magneto-convection results obtained by codes from several research groups [18].

The computational domain is discretized with high accuracy, utilizing approximately 20 million block-structured hexahedral cells. The topology of the mesh in a cross-sectional plane is shown in Fig. 3. The maximum cell size in the blocks resolving the core region of the cavity is set to 5×10^{-3} L. A nonuniform grid spacing towards the walls of the cavity provides high resolution of boundary layers δ_H and δ_s perpendicular and parallel to **B**. For $Ha = 1000$, δ_H is resolved by 7 layers and δ_s by more than 40. The region around the cooling pipe is resolved with a very fine radial-circumferential grid with 35 graded cells employed radially in the boundary layer δ_p.

Each simulation typically requires between 10 and 14 days to achieve converged temporal statistics, with significant performance enhancements facilitated by parallelization utilizing 960 processor cores on the CINECA MARCONI cluster.

3.1. Bifurcation from 2D to 3D

Given the assumption of an infinitely long domain in the x direction, the model problem is predisposed to generating two-dimensional solutions in planes of cross sections. In this context, 2D simulations [19] were performed with a short length in the x direction discretized into few axial cells, thereby effectively enforcing the two-dimensionality. Major results reveal that for a relatively small Grashof number ($Gr = 3.2\times10^6$), the temperature distribution closely resembles that of pure thermal conduction, with temperature gradient primarily oriented in the radial direction. On a global scale, some fluid in the colder regions around the pipe moves downward while fluid in warmer regions rises, driving the flow of liquid metal from hot to cold zones due to buoyancy forces. For large Hartmann numbers, the fluid motion is significantly suppressed by the Lorentz force and thin internal layers develop along magnetic field lines tangent to the pipe. As the Grashof number increases, buoyant forces gradually overcome the opposing Lorentz force, facilitating the development of larger convection rolls, leading to a stratified temperature field with hot fluid above the pipe and thin thermal boundary layers around the pipe. This 2D flow is invariant along the duct axis. It has no axial velocity component and streamlines remain exclusively in cross-sectional planes.

Magnetohydrodynamic flows become intrinsically three-dimen sional due to the complex interactions between the magnetic field and fluid motion when the Grashof number exceeds a critical value. 3D simulations have been conducted with a sufficiently discretized axial length of the model geometry $0 < x < 2$, employing cyclic boundary conditions. Time-dependent flow patterns were observed and identified through the simulations. Initially, 2D convection rolls form with their axes aligned with the axial direction, followed by the appearance of rolls aligned along a transverse axis, indicating a transition from a 2D to a 3D flow structure.

In order to characterize the phenomena of 3D flow patterns, we introduce the normalized vorticity vector

$$\mathbf{R} = \boldsymbol{\omega}/\omega,$$

where the vorticity $\boldsymbol{\omega} = \nabla\times\mathbf{u}$ is scaled by its magnitude ω. The components of **R** give an indication about the orientation of the convection rolls. For instance, in the case of pure 2D flow patterns, the normalized vorticity becomes $\mathbf{R} = (\pm1, 0, 0)$. For characterization of entire 3D flow structures, the absolute values of components are volume-averaged as $\langle|R_x|\rangle$, $\langle|R_y|\rangle$, $\langle|R_z|\rangle$, indicating proportions of the rotational intensity in each specific plane (with normal unit vectors $\hat{\mathbf{x}}$, $\hat{\mathbf{y}}$, $\hat{\mathbf{z}}$) relative to the total rotational intensity. This approach provides a normalized framework, enabling a quantitative and detailed analysis of the orientation and temporal evolution of rotational intensity across the three primary planes of motion.

As an example, components of **R** are plotted over time in Fig. 4 for a case with $Gr = 3.2\times10^9$ and $Ha = 200$. During the initial phase R_x dominates, with values close to 1, reflecting a strong contribution from convection rolls with coaxial axes aligned predominantly along the x direction. In the transition phase ($t = 100$–200), R_x decreases to 0.48, indicating a gradual reduction in the rotational intensity in the yz-plane. Simultaneously, R_z increases significantly, reaching approximately 0.66, reflecting an increasing dominance of the rotational intensity along magnetic field lines in the xy-plane. In the final phase, R_x and R_z stabilize close to 0.6 and 0.5, respectively, reflecting a

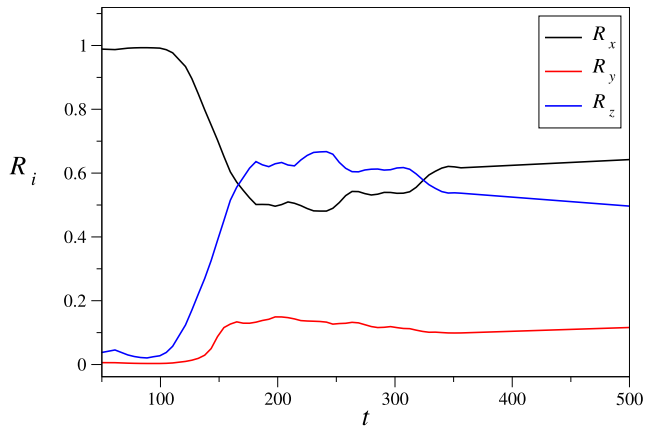

Fig. 4. Volume-averaged normalized absolute vorticity components over time for $Gr = 3.2 \times 10^9$ and $Ha = 200$.

coexistence of rotational intensity in both the yz-plane and xy-plane. A corresponding established flow pattern is shown in Fig. 5 (top). It is important to note that the results presented in Figs. 5–9 correspond to instantaneous data taken at a time, at which the convective roll patterns assumed converged statistics.

3.2. Influence of Ha on flow patterns

To gain a more comprehensive understanding of the influence of the Hartmann number on flow patterns, a systematic series of numerical simulations has been performed for $200 \leq Ha \leq 1000$ by keeping constant a relatively high Grashof number $Gr = 3.2 \times 10^9$ for which buoyancy-driven forces should dominate. These simulations offer detailed insights into the interaction between magnetic damping and flow dynamics, enabling a rigorous analysis of how variations in the Hartmann number affect flow structures and associated heat transfer mechanisms.

Fig. 5 illustrates the convective rolls present in the liquid metal flow, visualized through isosurfaces of the Q criterion [20]. The Q criterion is a vortex identification method in fluid dynamics, where Q is defined as $Q = \frac{1}{2}(\|\mathbf{\Omega}\|^2 - \|\mathbf{S}\|^2)$ and Ω and S are the rotational and strain rate tensors. Positive Q values indicate regions where rotational effects dominate over strain, signifying the presence of vortices. In Fig. 5 five values of Q, evenly spaced in the range from 0 to 1, are plotted. The isosurfaces of Q are colored by velocity magnitude, highlighting variations in flow intensity and enabling the identification of high-velocity regions.

In all cases, the region above the pipe remains nearly motionless, with no convection detected. For $Ha = 200$ convection rolls invariant in the x direction, are observed in the region adjacent to the pipe. In the lower section of the duct, small convective rolls with coaxial rotation axes emerge directly beneath the pipe. Additionally, small convective rolls with transverse rotation axes (z axis) develop near the bottom wall of the duct. These rolls interact with the larger convection rolls with coaxial rotation axes, resulting in a complex mixed structure in the lower section. For $Ha = 500$, convection rolls in the region adjacent to the pipe are smaller due to magnetic damping, compared to those observed at $Ha = 200$. In the lower section of the duct, only convective rolls with transverse rotation axes parallel to magnetic field lines are present. As the Hartmann number is increased further to $Ha = 1000$, the convection rolls continue to elongate in the direction of the magnetic field, with the size of the rolls increasing.

To facilitate a detailed examination, contours of velocity magnitude are presented in Fig. 6 for both the cross-sectional ($x = 0$) and longitudinal ($z = 0$) symmetry planes. For $Ha = 200$, the highest velocity is recorded directly beneath the pipe, with small rotational flow patterns

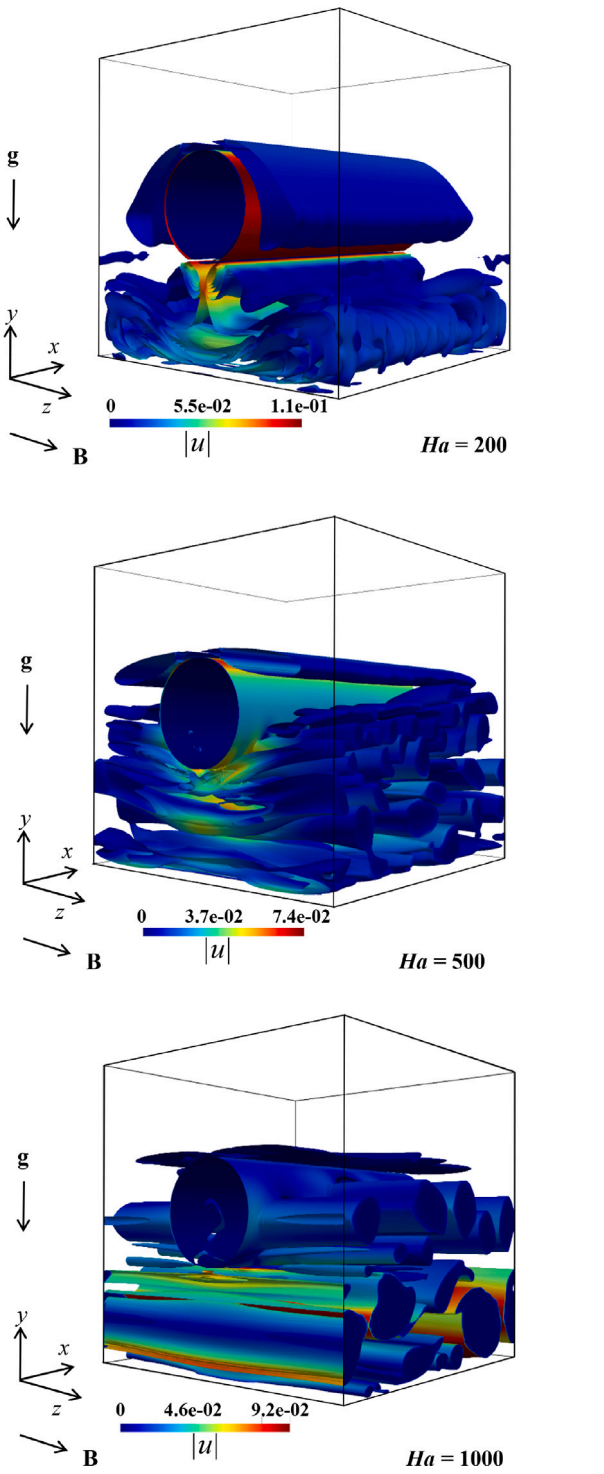

Fig. 5. Visualization of convective rolls using isosurfaces of Q, colored by velocity magnitude, for constant Grashof number $Gr = 3.2 \times 10^9$ and different Hartmann numbers: $Ha = 200$ (top), $Ha = 500$ (middle) and $Ha = 1000$ (bottom).

observed in the velocity field near the bottom wall of the duct. As the Hartmann number increases, the highest velocity occurs at the edges of the convective rolls and the size of the vortical structure increases. The velocity results align with the visualization of convective rolls, demonstrating how the magnetic field influences flow dynamics by promoting a more organized flow with vortices aligned preferentially along magnetic lines.

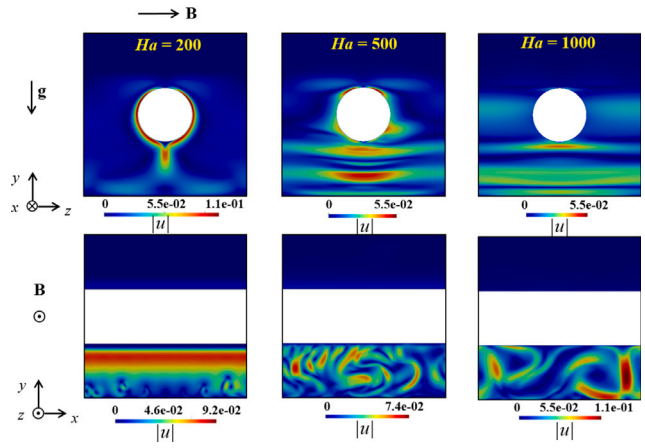

Fig. 6. Contours of velocity magnitude on the slice $x = 0$ (top) and $z = 0$ (bottom) for $Gr = 3.2 \times 10^9$ and different Hartmann numbers.

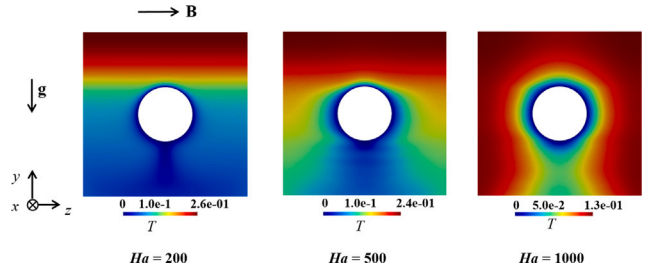

Fig. 7. Temperature contours in the slice $x = 0$ for $Gr = 3.2 \times 10^9$ and different Hartmann numbers.

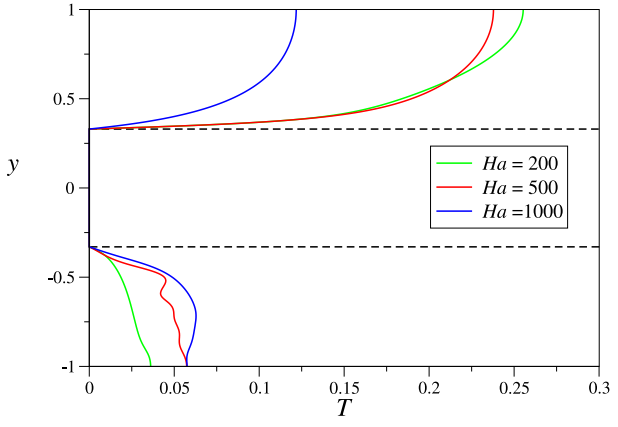

Fig. 8. Temperature profiles along the vertical y axis for or $Gr = 3.2 \times 10^9$ and different Hartmann numbers.

Convective rolls with transverse rotation axes contribute to enhanced mixing and localized heat transport, impacting the overall convective heat transfer, as illustrated by the temperature contours in Fig. 7 . With increasing Ha, the alignment and size of the convection rolls with transverse rotation axes are amplified. This enhancement promotes more efficient thermal mixing and lower maximum temperature, leading to a reduction in the stratification of the temperature field. In all cases, the highest temperatures are observed in the upper, almost motionless regions of the duct and the highest temperatures decrease with increasing Hartmann number. In order to emphasize this effect quantitatively, results for temperature are plotted along the y axis in a Fig. 8 for $Ha = 200$, 500, 1000.

In summary, with increasing Ha, we observe the formation of larger and more organized convection rolls, which align with the direction of the magnetic field. Consequently, the convection rolls improve thermal mixing, reducing thermal stratification. Additionally, the velocity reaches its maximum at the edges of the convection rolls, with velocity magnitude increasing with Ha.

3.3. Influence of Gr on flow patterns

In this section, the effects of varying the Grashof number Gr on flow patterns are systematically examined, with the Hartmann number $Ha = 1000$ held constant. A key observation is that at low Grashof number $Gr = 3.2 \times 10^6$, the flow remains two-dimensional (2D), with axes of convective rolls aligned exclusively along x-axis, as shown in Fig. 9. In this regime the buoyant forces, which are responsible for initiating three-dimensional structures, are not strong enough to overcome the suppression induced by the magnetic field, thus preventing the development of rolls in the transverse direction.

As the Grashof number increases, the velocity of the fluid also increases, driven by the strengthening buoyancy forces. The highest velocity is typically observed at the edges of the convective rolls, where the fluid experiences the greatest shear and accelerates as it moves through the convective structures. As the flow evolves, the convective rolls become more “turbulent” and complex, leading to enhanced mixing and more effective heat transfer.

3.4. Heat transfer

In classical Rayleigh–Bénard convection, the Nusselt number quantifies the enhancement of heat transfer through convection by comparing the mean heat flux in the convecting layer to that of assumed pure heat conduction. However, for systems with internal volumetric heating, where heat generation is uniformly distributed throughout the volume rather than governed by boundary-driven temperature gradients, the Nusselt number based on heat flux is inherently constant and therefore inadequate for describing the heat transfer dynamics. For volumetric heating, Roberts [21] introduced the modified Nusselt number:

$$M = \frac{T_{conduction}}{T_{convection}},$$

where $T_{conduction}$ is the volume-averaged temperature of the fluid in immobilized (pure conductive) state and $T_{convection}$ is the volume-averaged temperature where the fluid domain is under convection. The parameter M describes the thermal efficiency of convection relative to conduction, but from a mean temperature perspective rather than a flux perspective. Specifically, when convection enhances heat transfer, $T_{convection}$ will typically be lower than $T_{conduction}$, resulting in $M > 1$. In this study, $T_{conduction}$ is calculated for $\mathbf{u} = 0$, *i.e.* when there is no convection.

The modified Nusselt number M is plotted as a function of the Grashof number Gr for two Hartmann numbers Ha in Fig. 10 for 2D and 3D simulations. First, it can be observed that convective heat transfer increases with Gr and decreases with Ha, which aligns with the experimental results by Burr et al. [4,5]. Second, the heat transfer results further substantiate the observed flow pattern transitions. As the flow evolves from 2D to 3D configurations, a significant enhancement in convective heat transfer is observed, marked in the diagrams as “Bifurcation 2D→3D”. This increase in heat transfer efficiency is provoked by the formation of larger convection rolls with rotation axes aligned with the magnetic field, which enhance global fluid mixing. The transition to 3D flow, driven by an increase in buoyancy forces as Gr increases, plays a pivotal role in altering the thermal characteristics of the system, leading to a pronounced improvement in convective heat transfer. Interestingly, while the heat transfer in assumed 2D flow is strongly suppressed by increasing magnetic fields, the reduction of M with Ha is only moderate in case of 3D flows, where vortices may align with **B**.

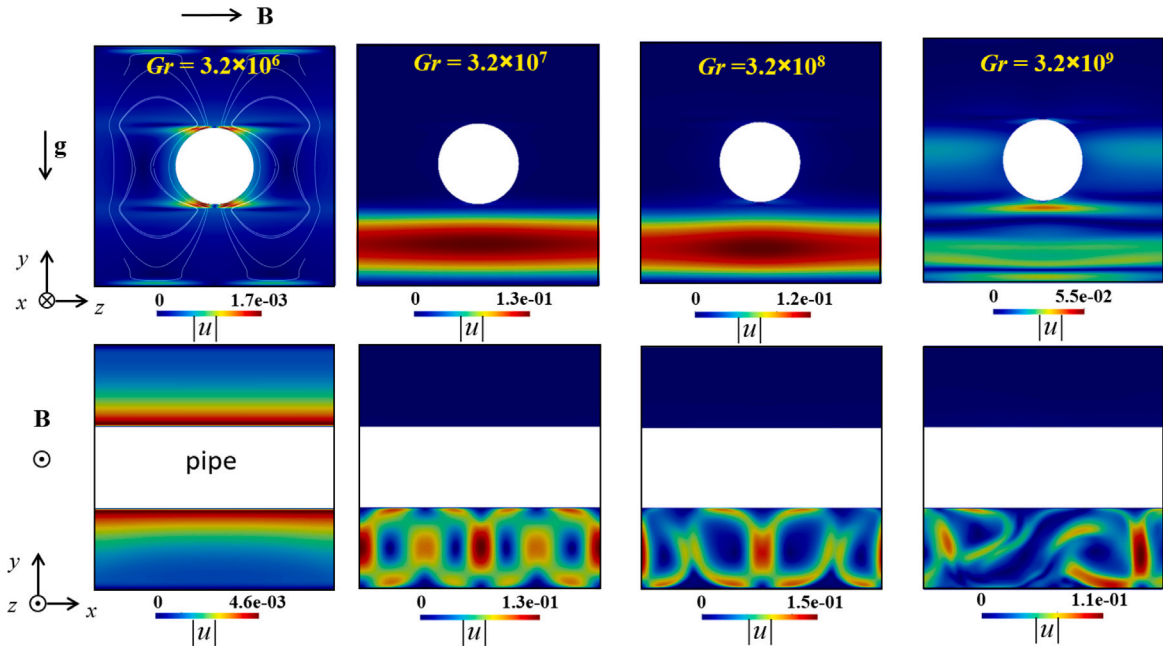

Fig. 9. Contours of velocity magnitude are shown for the slice $x = 0$ (top) and $z = 0$ (bottom) for $Ha = 1000$ and different Grashof numbers. For the 2D case at $Gr = 3.2 \times 10^6$, velocity streamlines have been overlaid for better understanding of the flow pattern.

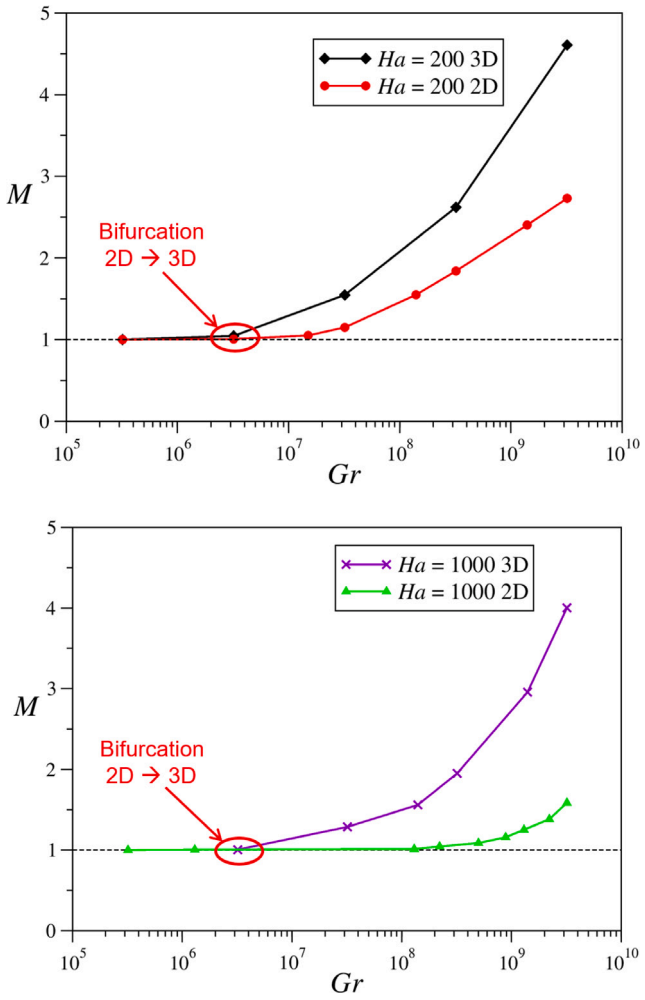

Fig. 10. Modified Nusselt number M as a function of the Grashof number Gr for $Ha = 200$ (upper) and $Ha = 1000$ (lower).

4. Conclusions

The present work investigates the MHD convective flow in a generic geometry associated with WCLL blankets, focusing on the development of three-dimensional magneto-convective instabilities and their impact on heat transfer.

The Hartmann number Ha characterizes the braking effect by the magnetic field, which suppresses flow motion, while the Grashof number Gr represents the driving mechanism by buoyancy, promoting fluid motion within the system. An increase in Ha intensifies the suppression of convection by the magnetic field, whereas higher Gr values amplify buoyancy effects, fostering the formation of larger convection rolls and enhancing heat transfer. The present study of heat transfer in volumetrically heated fluids reveals that when Ha is large and Gr is moderate, the magneto-convective flow remains predominantly two-dimensional (invariant along the x direction), resembling the behavior of pure conduction with minimal convection. When Gr exceeds a critical threshold, the flow transitions from two-dimensional structures to more complex three-dimensional patterns, with convection rolls preferentially aligning with the transverse magnetic field. This bifurcation from 2D to 3D flow patterns enhances heat transfer by facilitating larger flow structures with more effective convection with transverse rotation axes.

In previous theoretical and experimental analyses of heat transfer at differentially heated pipes [22,23] it was suggested that a combined parameter Gr/Ha^2 determines heat transfer in terms of a Nusselt number. Results of present simulations shown in Fig. 10 reveal, that the transition from 2D to 3D flow pattern is rather governed by the Grashof number Gr than by a combination with Ha. To identify the threshold for 2D to 3D transition, *i.e.* $Gr_c\,(Ha)$, additional simulations are required in future studies. A larger database is also required to derive the heat transfer correlation $M(Gr, Ha)$. Moreover, since the size of convective 3D flow patterns may depend on the axial length of the geometry, the latter parameter should be also varied in future simulations for confirming the observed scaling.

The present numerical simulations prove that the numerical code is capable of simulating magneto-convective flows with volumetric heat sources in strong magnetic fields and high Grashof numbers for a generic geometry relevant for WCLL blankets. Calculations for more realistic geometries and spatial distribution of power density will be conducted in future simulations.

CRediT authorship contribution statement

B. Lyu: Writing – original draft, Visualization, Validation, Software, Methodology, Investigation, Formal analysis, Data curation, Conceptualization. **L. Bühler:** Writing – review & editing, Resources, Funding acquisition, Conceptualization. **C. Koehly:** Software, Investigation, Data curation. **C. Mistrangelo:** Writing – review & editing, Software, Methodology, Investigation, Data curation, Conceptualization.

Declaration of competing interest

The authors declare that they have no known competing financial interests or personal relationships that could have appeared to influence the work reported in this paper.

Acknowledgments

This work has been carried out within the framework of the EUROfusion Consortium, funded by the European Union via the Euratom Research and Training Programme (Grant Agreement No 101052200 — EUROfusion). Views and opinions expressed are however those of the author(s) only and do not necessarily reflect those of the European Union or the European Commission. Neither the European Union nor the European Commission can be held responsible for them.

Data availability

Data will be made available on request.

References

[1] G. Federici, L. Boccaccini, F. Cismondi, M. Gasparotto, Y. Poitevin, I. Ricapito, An overview of the EU breeding blanket design strategy as an integral part of the DEMO design effort, Fusion Eng. Des. 141 (2019) 30–42, http://dx.doi.org/10.1016/j.fusengdes.2019.01.141.

[2] L. Boccaccini, U. Fischer, K. Kleefeldt, S. Malang, K. Schleisiek, Strategy for the blanket testing in ITER, Fusion Eng. Des. 61–62 (2002) 423–429.

[3] S. Chandrasekhar, Hydrodynamic and Hydromagnetic Stability, Dover Publications Inc., New York, 1961.

[4] U. Burr, U. Müller, Rayleigh-Bénard convection in liquid metal layers under the influence of a vertical magnetic field, Phys. Fluids 13 (11) (2001) 3247–3257, http://dx.doi.org/10.1063/1.1404385.

[5] U. Burr, U. Müller, Rayleigh-Bénard convection in liquid metal layers under the influence of a horizontal magnetic field, J. Fluid Mech. 453 (2002) 345–369, http://dx.doi.org/10.1017/S002211200100698X.

[6] O. Zikanov, I. Belyaev, Y. Listratov, P. Frick, N. Razuvanov, V. Sviridov, Mixed convection in pipe and duct flows with strong magnetic fields, Appl. Mech. Rev. 73 (2021) 010801–1–35, http://dx.doi.org/10.1115/1.4049833.

[7] Y. Yan, A. Ying, M. Abdou, Numerical study of magneto-convection flows in a complex prototypical liquid-metal fusion blanket geometry, Fusion Eng. Des. 159 (2020) 111688, http://dx.doi.org/10.1016/j.fusengdes.2020.111688.

[8] L. Chen, X. Zheng, M. Ni, Numerical study of MHD mixed convection flow in the EU DEMO WCLL breeding blanket, Fusion Eng. Des. 194 (2023) 113906, http://dx.doi.org/10.1016/j.fusengdes.2023.113906.

[9] F.R. Urgorri, I. Fernández-Berceruelo, D. Rapisarda, Magneto-convective analyses of the PbLi flow for the EU-WCLL fusion breeding blanket, Energies 14 (19) (2021) http://dx.doi.org/10.3390/en14196192.

[10] P. Arena, A. Del Nevo, F. Moro, S. Noce, R. Mozzillo, V. Imbriani, F. Giannetti, F. Edemetti, A. Froio, L. Savoldi, S. Siriano, A. Tassone, F. Roca Urgorri, P.A. Di Maio, I. Catanzaro, G. Bongiovi, The DEMO water-cooled lead-lithium breeding blanket: design status at the end of the pre-conceptual design phase, Appl. Sci. 11 (24) (2021) http://dx.doi.org/10.3390/app112411592.

[11] A. Del Nevo, P. Arena, G. Caruso, P. Chiovaro, P.D. Maio, M. Eboli, F. Edemetti, N. Forgione, R. Forte, A. Froio, F. Giannetti, G. Di Gironimo, K. Jiang, S. Liu, F. Moro, R. Mozzillo, L. Savoldi, A. Tarallo, M. Tarantino, A. Tassone, M. Utili, R. Villari, R. Zanino, E. Martelli, Recent progress in developing a feasible and integrated conceptual design of the WCLL BB in EUROfusion project, Fusion Eng. Des. 146 (2019) 1805–1809, http://dx.doi.org/10.1016/j.fusengdes.2019.03.040.

[12] J. Aubert, G. Aiello, D. Alonso, T. Batal, R. Boullon, S. Burles, B. Cantone, F. Cismondi, A. Del Nevo, L. Maqueda, A. Morin, E. Rodríguez, F. Rueda, M. Soldaini, J. Vallory, Design and preliminary analyses of the new Water Cooled Lithium Lead TBM for ITER, Fusion Eng. Des. 160 (2020) 111921, http://dx.doi.org/10.1016/j.fusengdes.2020.111921.

[13] R. Mößner, U. Müller, A numerical investigation of three-dimensional magnetoconvection in rectangular cavities, Int. J. Heat Mass Transfer 42 (6) (1999) 1111–1121, http://dx.doi.org/10.1016/S0017-9310(98)00115-X.

[14] L. Bühler, C. Mistrangelo, MHD flow and heat transfer in model geometries for WCLL blankets, Fusion Eng. Des. 122 (2017) 919–923, http://dx.doi.org/10.1016/j.fusengdes.2017.01.014.

[15] C. Mistrangelo, L. Bühler, Development of a numerical tool to simulate magneto-hydrodynamic interactions of liquid metals with strong applied magnetic fields, Fusion Sci. Technol. 60 (2) (2011) 798–803, http://dx.doi.org/10.13182/FST11-A12483.

[16] M.-J. Ni, R. Munipalli, P. Huang, N.B. Morley, M.A. Abdou, A current density conservative scheme for incompressible MHD flows at a low magnetic Reynolds number. Part II: On an arbitrary collocated mesh, J. Comput. Phys. 227 (1) (2007) 205–228, http://dx.doi.org/10.1016/j.jcp.2007.07.023.

[17] C. Mistrangelo, L. Bühler, H.-J. Brinkmann, C. Courtessole, V. Klüber, C. Koehly, Magneto-convective flows around two differentially heated cylinders, Heat Mass Transf. 59 (2023) 2005–2021, http://dx.doi.org/10.1007/s00231-023-03350-2.

[18] S. Smolentsev, T. Rhodes, Y. Yan, A. Tassone, C. Mistrangelo, L. Bühler, F.R. Urgorri, Code-to-code comparison for a PbLi mixed-convection MHD flow, Fusion Sci. Technol. 76 (2020) 653–669, http://dx.doi.org/10.1080/15361055.2020.1751378.

[19] C. Mistrangelo, L. Bühler, C. Koehly, Considerations on magneto-convective flows in model geometries relevant for fusion applications, in: Proceedings of the 11th International PAMIR Conference - Fundamental and Applied MHD, July 01 - 05, 2019, Reims, France, 2019, pp. 7–11.

[20] J.C.R. Hunt, A. Wray, P. Moin, Eddies, streams, and convergence zones in turbulent flows, in: Proceeding, of the Summer Program 1988, Center for Turbulence Research, 1988, pp. 193–208.

[21] P.H. Roberts, Convection in horizontal layers with internal heat generation. Theory, J. Fluid Mech. 30 (1) (1967) 33–49, http://dx.doi.org/10.1017/S0022112067001284.

[22] C. Mistrangelo, L. Bühler, C. Courtessole, Numerical and experimental analysis of magneto-convective flows around pipes, Fusion Eng. Des. 202 (2024) 113425, http://dx.doi.org/10.1016/j.fusengdes.2024.114325.

[23] C. Courtessole, H.-J. Brinkmann, L. Bühler, Experimental investigation of magneto-convective flows around two differentially heated cylinders, J. Fluid Mech. 993 (2024) A6–1 – A6–22, http://dx.doi.org/10.1017/jfm.2024.591.